Title

Kinetic investigation reveals an HIV-1 Nef-dependent increase in AP-2 recruitment and productivity at endocytic sites

Journal

Molecular Biology of the Cell, 35(1)

ISSN

1059-1524

Authors

Iwamoto, Yuichiro

Ye, Anna A

Shirazinejad, Cyna

et al.

Publication Date

2024

DOI

10.1091/mbc.e23-04-0126

Peer reviewed

Kinetic investigation reveals an HIV-1 Nef-dependent increase in AP-2 recruitment and productivity at endocytic sites

Yuichiro Iwamoto[a], Anna A. Ye[a], Cyna Shirazinejad[c], James H. Hurley[a,b,c,d,*], and David G. Drubin[a,b,c,*]
[a]Department of Molecular and Cell Biology, [b]California Institute for Quantitative Biosciences, [c]Biophysics Graduate Group, and [d]Helen Wills Neuroscience Institute, University of California, Berkeley, Berkeley, CA 94720

ABSTRACT **The HIV-1 accessory protein Nef hijacks clathrin adaptors to degrade or mislocalize host proteins involved in antiviral defenses. Here, using quantitative live-cell microscopy in genome-edited Jurkat cells, we investigate the impact of Nef on clathrin-mediated endocytosis (CME), a major pathway for membrane protein internalization in mammalian cells. Nef is recruited to CME sites on the plasma membrane, and this recruitment is associated with an increase in the recruitment and lifetime of the CME coat protein AP-2 and the late-arriving CME protein dynamin2. Furthermore, we find that CME sites that recruit Nef are more likely to recruit dynamin2 and transferrin, suggesting that Nef recruitment to CME sites promotes site maturation to ensure high efficiency in host protein downregulation. Implications of these observations for HIV-1 infection are discussed.**

Monitoring Editor
Jennifer Lippincott-Schwartz
Howard Hughes Medical Institute

Received: Apr 14, 2023
Revised: Oct 24, 2023
Accepted: Nov 2, 2023

SIGNIFICANCE STATEMENT

- HIV protein Nef interacts with the clathrin-mediated endocytosis pathway of the infected host to internalize host proteins from the cell surface.
- The spatiotemporal kinetics of this process has not been thoroughly studied. With TIRF and HILO microscopy, the authors image the Nef-dependent changes in the dynamics of the host clathrin-mediated endocytosis pathway.
- They report Nef-dependent increase in endocytic coat protein AP-2 accumulation and lifetime, as well as an increase in the productivity of endocytic sites that recruit Nef. The results of this study suggest Nef may increase the productivity of endocytic sites, a previously unappreciated function that may aid downregulation.

This article was published online ahead of print in MBoC in Press (http://www.molbiolcell.org/cgi/doi/10.1091/mbc.E23-04-0126) on November 8, 2023.

Competing interest statement: J.H.H. is a cofounder of Casma Therapeutics and receives research funding from Genentech and Hoffmann-La Roche. The other authors declare no competing interests.

*Address correspondence to: James H. Hurley (jimhurley@berkeley.edu); David G. Drubin (drubin@berkeley.edu).

Abbreviations used: CME, clathrin-mediated endocytosis; DNM2, dynamin2; HILO, highly inclined and laminated optical sheet

INTRODUCTION

Human immunodeficiency virus (HIV) depends on accessory viral proteins for its efficient replication and spread (Collins and Collins, 2014). HIV accessory proteins, including Nef, Vpu, Vif, Vpr, and Vpx, counteract host defenses by redirecting cellular pathways for the benefit of the virus (Malim and Bieniasz, 2012; Collins and Collins, 2014).

Here, we focus on the protein Nef, a nonenzymatic accessory protein encoded in the HIV genome (Allan *et al.*, 1985). A major function of Nef is to downregulate host transmembrane proteins involved in antiviral restriction and immune response (Pereira and daSilva, 2016; Buffalo *et al.*, 2019a). Numerous studies support Nef's significant role in enhancing HIV infection (Kestler *et al.*, 1991; Deacon *et al.*, 1995; Kirchhoff *et al.*, 1995; Basmaciogullari and Pizzato, 2014).

Well-established targets or cargo for HIV-1 Nef downregulation include the host membrane proteins CD3, CD4, CD28, MHC-I, and SERINC3/5 (Pereira and daSilva, 2016; Buffalo *et al.*, 2019a). Of relevance to the current study, Nef downregulates the CD4 receptor (Guy *et al.*, 1987; Inoue *et al.*, 1993; Aiken *et al.*, 1994) and the restriction factors SERINC3/5 (Rosa *et al.*, 2015; Usami *et al.*, 2015) and tetherin (in SIV but not HIV) (Jia *et al.*, 2009; Zhang *et al.*, 2009; Serra-Moreno *et al.*, 2013) from the plasma membrane in a CME-dependent manner. Notably, the Nef-dependent infectivity enhancement of HIV-1 in cultured cells is almost completely recapitulated by SERINC3/5 knockout, identifying SERINC3/5 downregulation as a critical component of Nef function (Usami *et al.*, 2015). Thus, complete understanding of how Nef contributes to viral infection requires investigation of Nef's effects on CME.

Much of our current understanding of how Nef modulates the CME pathway in cells comes from flow cytometry studies measuring Nef-related cargo downregulation and from immunofluorescence studies of Nef and CME protein localization. These studies revealed that Nef and its cargo are recruited to CME sites and that Nef downregulates cargo proteins such as CD4 and MHC-I over the time scale of hours (Aiken *et al.*, 1994; Schwartz *et al.*, 1996; Greenberg *et al.*, 1997). Though informative, the methods employed fail to capture Nef and CME protein dynamics during individual endocytic events, which occur on the minute timescale. Research in yeast and mammals has revealed that a well-orchestrated recruitment sequence for over 60 proteins can be observed in this short time window, and that the dynamics of these endocytic proteins can sensitively detect pathway alterations and their causes (Taylor *et al.*, 2011; Lu *et al.*, 2016).

Specifically, the relationship between the dynamics of AP-2, a major protein component present in most clathrin-coated pits (Boucrot *et al.*, 2010), and the CME pathway has been addressed through numerous studies. Mutations that result in impaired ability of AP-2 to bind to lipid bilayers result in formation of fewer CME events, lower accumulation of AP-2 at CME sites, and an increase of short-lived clathrin-coated structures that may represent aborted endocytic events (Kadlecova *et al.*, 2017). On the other hand, productive CME events, which culminate in successful clathrin-coated vesicle internalization, are characterized by higher amounts and longer accumulation of AP-2 and clathrin (Hong *et al.*, 2015; He *et al.*, 2020). The ratio of AP-2 to clathrin has been suggested to determine the timing of the clathrin-coat curvature development, which may mark an important regulatory transition point in the CME pathway (Bucher *et al.*, 2018). Together, these findings suggest that proper AP-2 recruitment is important for CME function, and that insights into how perturbations to CME affect this process can be gleaned by quantitative analysis of AP-2 dynamics in live cells.

That AP-2 is required for the Nef-dependent cargo downregulation via CME is well established (Jin *et al.*, 2005; Chaudhuri *et al.*, 2007). Nef interacts with AP-2 directly via an acidic dileucine motif in a flexible disordered loop (Ren *et al.*, 2014). This interaction occurs in a similar manner to how AP-2 interacts with cellular cargo proteins as the Nef dileucine motif is similar to those found in cellular transmembrane proteins such as LDLR (Kelly *et al.*, 2008; Ren *et al.*, 2014). In addition, structures of Nef complexed with AP-2 and the Nef-binding cytosolic tail of downregulated host factors have been solved (Buffalo *et al.*, 2019b; Kwon *et al.*, 2020). These structural findings led to our current model in which CME hijacking by Nef occurs when Nef acts as an adaptor for AP-2, linking the downregulated cargo to AP-2, and thereby the CME pathway, for internalization.

Given that AP-2 interacts with Nef directly, and given the sensitivity of CME to AP-2 dynamics, we hypothesized that Nef modulates the CME pathway through binding to AP-2. A previous study conducted by Burtey *et al.* (2007) revealed that Nef and clathrin dynamics at CME sites can be monitored on the plasma membrane through total internal reflection fluorescence microscopy (TIRF) in live cells. Utilizing this method, the study revealed that dileucine motif-dependent recruitment of Nef to CME sites is linked to Nef's ability to downregulate CD4 (Burtey *et al.*, 2007). Here, by monitoring AP-2 dynamics in genome-edited cells that express this protein and dynamin 2 (DNM2) as fluorescent protein fusions at endogenous levels, and utilizing present-day, advanced particle tracking analysis, we aim to elucidate previously unappreciated effects of Nef on the CME pathway. To accurately detect Nef-dependent changes in CME dynamics, we employ Jurkat cells, which are immortalized human T cells (Schwenk and Schneider, 1975; Abraham and Weiss, 2004). We opted to primarily use the HIV-1 NA7 Nef patient isolate because it is a natural HIV-1 allele that has been shown to potently promote CD4 internalization (Mariani and Skowronski, 1993; Mariani *et al.*, 1996). NA7 Nef is also medically relevant because this allele was isolated from an HIV-1 group M virus, which is by far the most predominant type of HIV associated with human infections.

Here, our quantitative CME dynamics analysis reveal Nef-dependent changes to AP-2 dynamics. These changes in AP-2 dynamics rely on the Nef dileucine motif, which is the primary AP-2 binding domain of Nef. Additionally, CME sites that recruit Nef appear to have increased productivity, a previously unappreciated function of Nef that may further enhance the efficiency of host defense factor downregulation through the CME pathway.

RESULTS

CME dynamics in genome-edited Jurkat cells

To develop a cell line that would allow us to investigate whether HIV Nef affects CME dynamics, we genome-edited Jurkat cells, a T-cell leukemia cell line that resembles natural HIV hosts (Schwenk and Schneider, 1975; Abraham and Weiss, 2004). The resulting line stably expresses fluorescent protein-tagged endocytic proteins at endogenous levels. These cells were engineered to express the endocytic adapter protein AP-2 labeled with tagRFPt, and the late arriving scission factor dynamin 2 labeled with EGFP (Supplemental Figures S1, A and B; Doyon *et al.*, 2011; Hong *et al.*, 2015). AP-2 is both a direct binding partner of Nef and an established marker for most CME events that is present at CME sites for much if not all of clathrin-coat assembly (Boucrot *et al.*, 2010; Cocucci *et al.*, 2012). DNM2 serves as marker for vesicle scission (Merrifield *et al.*, 2002; Cocucci *et al.*, 2014; Grassart *et al.*, 2014; Antonny *et al.*, 2016; Supplemental Figure S1F). Both proteins localize to punctate structures on the plasma membrane, marking sites of endocytosis (CME sites). As expected, AP-2 and DNM2 colocalized at punctate, cortical patches (Figure 1, A and C).

Two imaging modalities were used in this study. The first is TIRF microscopy, which allows quantitative and sensitive imaging within ~250 nm of the cell-substrate interface, facilitating selective visualization of CME at a cell's basal membrane (Merrifield *et al.*, 2002). However, CME at the cell-substrate interface could be affected by factors such as substrate adhesion and membrane tension (Batchelder and Yarar, 2010). To analyze CME at nonadhered surfaces, we also employed a complementary imaging method, HILO microscopy (Tokunaga *et al.*, 2008), to image the medial focal plane of cells, similar to what is done commonly with yeast cells (Kaksonen *et al.*, 2003). We opted for HILO microscopy over conventional confocal microscopy for this purpose due to the high signal-to-noise

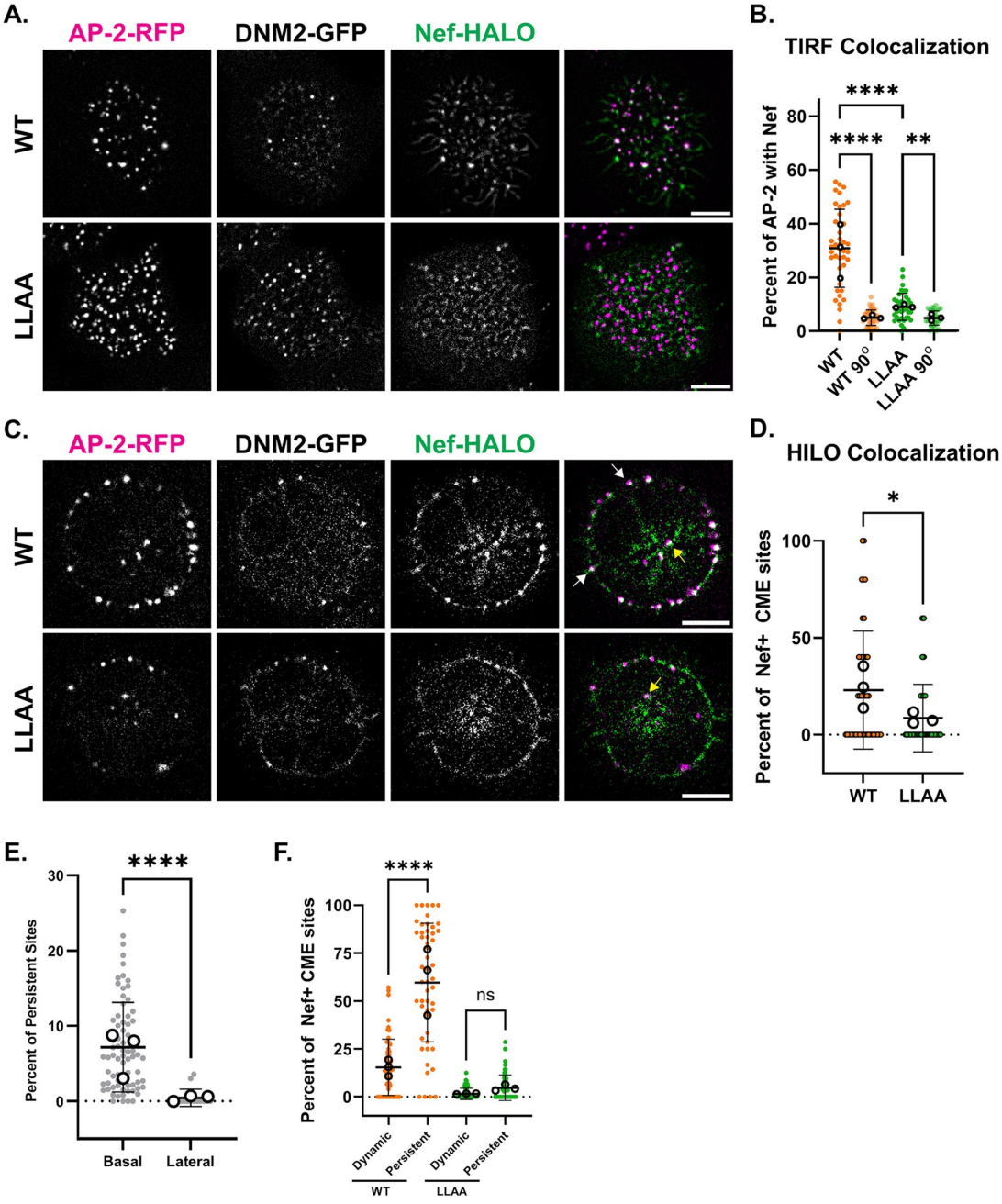

FIGURE 1: Recruitment of HIV Nef to CME sites. (A) TIRF image of Jurkat cells endogenously expressing AP-2-RFP, DNM2-GFP, and transfected overnight with a construct expressing WT or LLAA Nef-HALO. Local background was reduced by subtracting the median filtered image to highlight punctate structures. Scale bar is 5 μm. (B) Quantification of the colocalization between AP-2 and WT/LLAA Nef observed in TIRF movie. WT/LLAA 90° conditions represent when reference images were rotated 90° to estimate random colocalization. The percentage of AP-2 pixels that overlap with Nef signal is plotted. Each point represents a cell. Each open circle represents the mean value from a single biological replicate. Bars indicate SD. **, **** indicates p value between 0.01 – 0.001 and < 0.0001, respectively. (C) Midfocal plane image of Jurkat cells endogenously expressing AP-2-RFP and DNM2-GFP and transfected overnight with a construct expressing WT or LLAA Nef-HALO. Images were acquired through highly inclined and laminated optical sheet (HILO) microscopy. Local background was reduced by subtracting the median filtered image to highlight punctate structures. White arrows indicate cortical colocalization events. Yellow arrows indicate intracellular colocalization events. Scale bar is 5 μm. (D) Quantification of the colocalization between AP-2 and WT/LLAA Nef observed in HILO movie. Percentage of AP-2 puncta that colocalize with Nef was manually quantified and plotted. Each datapoint represents a cell. Each open circle represents the mean value from a single biological replicate. Bars indicate SD. * indicates p value between 0.01 – 0.05. (E) Quantification of the percentage of persistent AP-2 events on the membrane regions in contact or not in contact with the cover glass. Each datapoint represents a cell. Each open circle represents the mean value from a single biological replicate. Bars indicate SD. **** indicates $p < 0.0001$. (F) Quantification of the colocalization of WT/LLAA Nef in dynamic and persistent AP-2 sites from TIRF movies. Each datapoint represents a cell. Each open circle represents the mean value from a single biological replicate. Bars indicate SD. **** indicates $p < 0.0001$ and ns indicates $p \geq 0.05$.

ratio and low photobleaching offered by the method (Tokunaga *et al.*, 2008).

We primarily focused on two parameters to monitor CME dynamics. First, we quantified the maximum fluorescence intensity of CME proteins at each CME site to compare the levels of protein recruitment between different conditions. Second, we measured the lifetime, or the duration of time that signal from these proteins could be consecutively detected from a single punctate structure, to estimate the duration of CME events. Importantly, lifetime refers to the duration during which fluorescence from a tagged protein is detectable at a single CME site, rather than the duration of time a single molecule of the tagged proteins is present at the CME site.

Evidence that Nef is recruited to CME sites in Jurkat cells via interaction with AP-2

Utilizing genome-edited cells, we first investigated whether Nef is recruited to CME sites via interaction with AP-2. Nef contains an AP-2-binding dileucine motif shown previously by both live-cell imaging and fixed-cell immunostaining to be required for its efficient recruitment to CME sites (Greenberg *et al.*, 1997; Burtey *et al.*, 2007). To test whether this motif is also required for Nef recruitment to CME sites in Jurkat cells, we transfected the genome-edited Jurkat cells with either WT Nef or the dileucine motif LLAA mutant Nef. To examine Nef recruitment at the membrane, Nef localization was assessed through both TIRF and HILO microscopy (Figure 1, A and C; Supplemental Movie 2–5). TIRF microscopy results indicated that WT Nef was present at 31 ± 15% of AP-2 pixels while LLAA Nef was detectable at only 9 ± 5% of AP-2 pixels (Figure 1B). The chance localization of Nef at AP-2 was estimated by rotating the AP-2 image 90 degrees and quantifying colocalization with the unrotated Nef image. Both WT and LLAA Nef show greater colocalization in nonrotated images compared with random colocalization in the rotated images, indicating significant colocalization of WT and LLAA Nef with AP-2 (Figure 1B). For AP-2 sites on the portion of membrane not attached to the cover glass, WT Nef was detected at 23 ± 30% of AP-2 sites while LLAA Nef was only detected at 8 ± 17% of AP-2 sites (Figure 1D). Notably, the AP-2 sites could be categorized into dynamic events, appearing and disappearing within minutes, and persistent events, lasting the entire duration of the acquired movie. Strikingly, there were very few persistent AP-2 sites observed on the portion of the membrane not attached to the cover glass (Figure 1E). Persistent AP-2 sites were mostly observed in TIRF movies and exhibited increased dileucine dependent colocalization with Nef (60 ± 31%) compared with that of dynamic sites (15 ± 15%; Figure 1F). Because persistent CME events are much brighter than dynamic events, it is unlikely that the lack of persistent AP-2 events on the portion of the membrane not attached to the cover glass stems from sensitivity differences between HILO and TIRF microscopy (Supplemental Figure S2B). Both approaches confirm that Nef localizes to CME sites in a dileucine motif-dependent manner across different plasma membrane domains. Furthermore, these results suggest that Nef localization to CME sites is affected by contact between substrate and the plasma membrane, because increased colocalization between Nef and AP-2 was observed at persistent AP-2 events on the portion of membrane attached to the cover glass.

Unexpectedly, we also observed that Nef and AP-2 colocalized at intracellular structures. These structures likely reflect at least two types of Nef-AP-2 interactions. Some such structures are presumably recently internalized clathrin-coated vesicles that have not yet been uncoated because they resemble CME sites in intensity. However, other structures appear to be much brighter and larger in size than cortical endocytic sites (Figure 1C; Supplemental Movie 4). The intracellular structures exhibiting Nef-AP-2 colocalization were also observed in cells expressing LLAA Nef (Figure 1C). The nature of this second class of structure is presently unknown but may represent interactions between AP-2 and Nef at any of several organelles that Nef associates with (Pereira and daSilva, 2016).

Nef is recruited to CME sites early with similar dynamics to AP-2

We next investigated the kinetics of Nef recruitment to CME sites in TIRF movies. Kymograph analysis, which shows the intensity change over time, revealed that Nef colocalizes with AP-2 throughout the duration of the CME event (Figure 2A). The dynamics of Nef recruitment to CME sites were monitored quantitatively using cmeAnalysis, a particle tracking package for analyzing CME protein dynamics (Aguet *et al.*, 2013). We validated our analysis pipeline for CME events and Nef colocalization in TIRF movies by confirming that the analysis reported a similar degree of colocalization between WT Nef and AP-2 at dynamic CME sites as seen through HILO microscopy, while reporting reduced colocalization between LLAA Nef and AP-2 (Figure 1F). We focused on dynamic events because persistent events are rarely observed on the portion of membrane not attached to the cover glass. We determined that 15% of basal CME sites were Nef positive in WT Nef-transfected cells, while only 1.6% were Nef positive in LLAA Nef-transfected cells (Figure 1F).

Averaging the intensity change over time for CME proteins AP-2 and DNM2, as well as Nef, we verified our qualitative kymograph observations that Nef accumulates at CME sites over time and persists until presumed CME vesicle scission indicated by a prominent DNM2 peak (Figure 2B). The intensity increase of Nef over time resembles that of AP-2, consistent with Nef primarily interacting with AP-2 to modulate CME (Figure 2B; Supplemental Figure S2D). To assess the timing of Nef recruitment, we averaged the time between the first AP-2 and the first Nef detection across all CME sites to which Nef was recruited (Figure 2C). On average, Nef is first detected 18 s after AP-2 in these events (Figure 2C). We also measured the recruitment timing of DNM2, which has been shown previously to be recruited early at low levels during CME (Loerke *et al.*, 2009). DNM2 was detected 26 s after AP-2 on average, indicating that Nef arrives around when DNM2 is first detected (Figure 2C). Given these observations, we conclude that Nef is recruited to CME sites early, likely a short time after AP-2.

By tracking Nef puncta, we determined that less than 5% of detected Nef puncta were AP-2 positive in both WT and LLAA Nef-expressing Jurkat cells (Figure 2D). The lifetime of WT Nef at AP-2–positive events was 57 ± 36 s while the lifetime of LLAA Nef was 42 ± 28 s (Figure 2E). The max intensity of WT Nef and LLAA Nef puncta were similar (Figure 2E). The similarity of both lifetime and maximum intensity of WT and LLAA Nef at CME sites further support the conclusion that LLAA Nef can still be recruited to CME sites, though to a much lower percentage of events. The lifetime and maximum intensity of puncta only exhibiting Nef signal were similar regardless of whether WT or LLAA Nef was expressed (Figure 2F). Interestingly, the max intensity recorded from WT Nef-only puncta showed a much greater variance than LLAA Nef-only puncta, though the mean maximum intensity values were not significantly different. The density of these Nef-only punctate structures was comparable regardless of whether WT or LLAA Nef was being expressed (Figure 2G).

Nef recruitment appears to increase AP-2 lifetime at CME sites

To test for possible effects of Nef recruitment on the dynamics of CME proteins at endocytic sites, we classified CME events into three

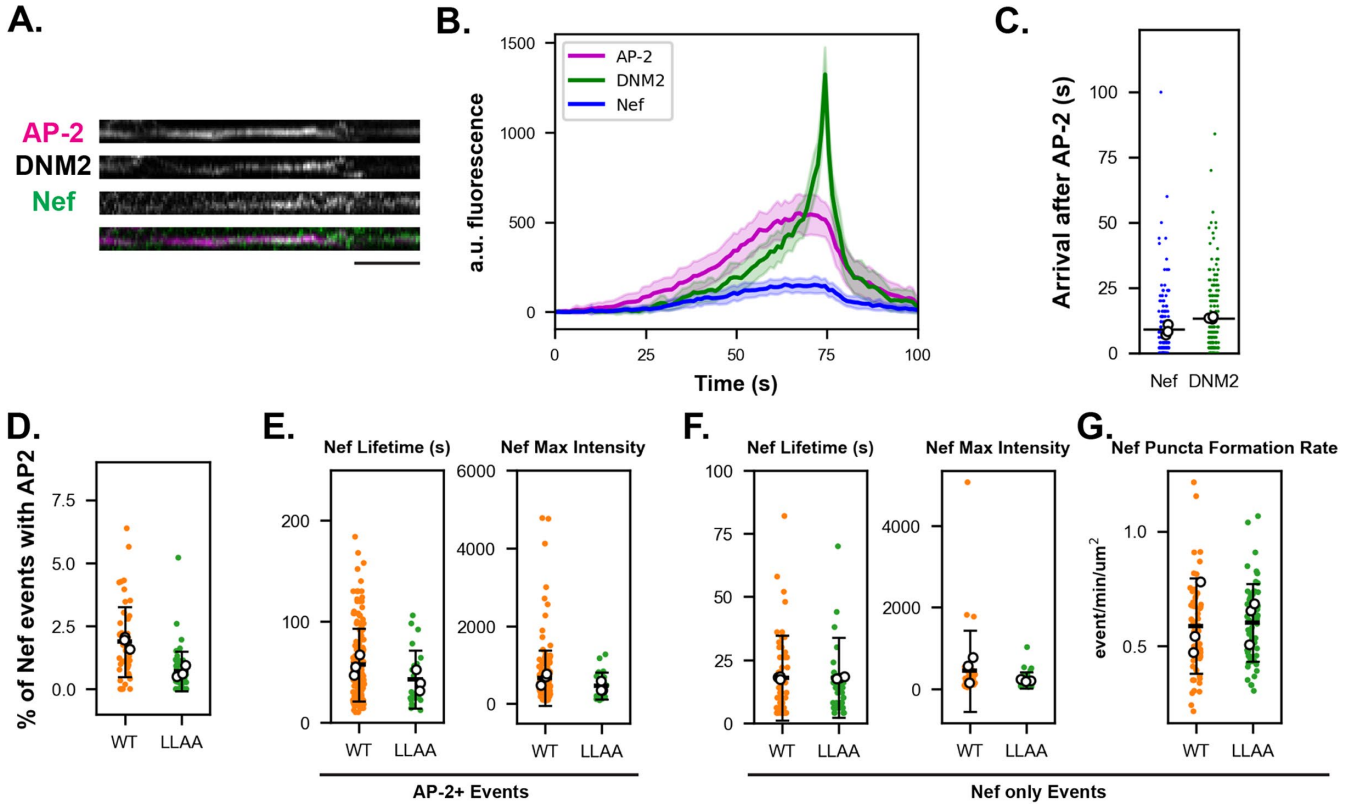

FIGURE 2: Nef is recruited early to CME sites with similar dynamics to AP-2. (A) Kymograph from a 5-min movie of a single Nef+ CME site in AP-2-RFP, DNM2-GFP Jurkat cells transfected with WT Nef-HALO. Scale bar is 1 min. (B) Graph showing the fluorescence intensity over time of averaged Nef-positive CME events with an AP-2 lifetime between 0–150 s. Outer lines of the curve represent standard deviations. Tracks were aligned to the maximum intensity of DNM2. (C) Quantification of time of first detection of Nef and DNM2 in Nef+ events after the first AP-2 detection. The black line indicates mean values. Each datapoint is a tracked Nef spot. Each open circle represents the mean value from a single biological replicate. (D) Quantification of the percentage of Nef puncta that colocalized with AP-2 (AP-2–positive puncta). Each datapoint is a tracked Nef spot. Each open circle represents the mean value from a single biological replicate. Bars indicate SD. (E) Quantification of Nef lifetimes and Nef maximum intensity in AP-2–positive Nef puncta. Each datapoint is a tracked Nef spot. Each open circle represents the mean value from a single biological replicate. Bars indicate SD. (F) Quantification of Nef lifetimes and max intensity in AP-2–negative Nef puncta. Each datapoint is a tracked Nef spot. Each open circle represents the mean value from a single biological replicate. Bars indicate SD. (G) Quantification of the formation rate of Nef puncta. Each datapoint is an individual cell. Each open circle represents the mean value from a single biological replicate. Bars indicate SD.

categories. The control category represents CME dynamics measured in untransfected AP-2-RFP DNM2-GFP Jurkat cells. The Nef+ and Nef– categories refer to CME sites in Nef-expressing cells that do and do not recruit Nef, respectively. Because substrate adhesion may alter CME dynamics, we chose to first analyze the effect of Nef on CME dynamics via HILO microscopy. To quantify CME dynamics at many CME sites, we generated kymographs around the circumference of these cells imaged through their medial focal planes (Supplemental Figure S2A). We quantified the lifetime over which the fluorescent proteins were detected on the cell periphery in these kymographs (Supplemental Figure S2C). The lifetime analysis revealed that CME sites in untransfected cells or at sites of transfected cells that lack detectable Nef exhibited similar AP-2 lifetimes of 66 ± 21 and 64 ± 19 s, respectively, while Nef+ CME sites exhibited longer AP-2 lifetimes averaging 87 ± 23 s (Supplemental Figure S2E). The LLAA Nef+ and Nef– CME sites displayed very similar lifetimes of 66 ± 28 and 65 ± 24 s, respectively, showing no statistically significant change in AP-2 lifetime (Supplemental Figure S2E). These results suggest that WT Nef recruitment to CME sites increases their lifetime.

Increased AP-2 and DNM2 recruitment and lifetimes observed at Nef+ CME sites by TIRF microscopy

We utilized the cmeAnalysis particle tracking software to analyze the effects of Nef recruitment to CME sites on dynamics of CME proteins. As with HILO imaging, we observed that Nef+ sites exhibit increased AP-2 lifetimes compared with control sites or Nef– sites (control 83 ± 41 s, WT Nef- 79 ± 44 s, WT Nef+ 110 ± 47 s; Figure 3A). Additionally, we noticed that the difference between AP-2 lifetimes for LLAA Nef+ events and for LLAA Nef– events was much smaller (LLAA Nef- 81 ± 41 s, LLAA Nef+ 89 ± 41 s; Figure 3A), suggesting that Nef's dileucine motif is important for its effects on CME dynamics, as for its recruitment to CME sites. Additionally, we quantified the maximum fluorescence intensity (max intensity) of AP-2 to test for effects of Nef recruitment. Nef+ CME sites showed increased AP-2 recruitment compared with Nef– and control CME sites (control 586.7 ± 439.1 au, Nef- 588.7 ± 470.4 au, Nef+ 877.2 ± 536.4 au; Figure 3B). In contrast, LLAA Nef+ sites showed little to no change compared with control or LLAA Nef- CME sites in AP-2 lifetime and recruitment (Figure 3B). Interestingly, similar increases in lifetime but not recruitment at Nef+ sites were also observed for DNM2

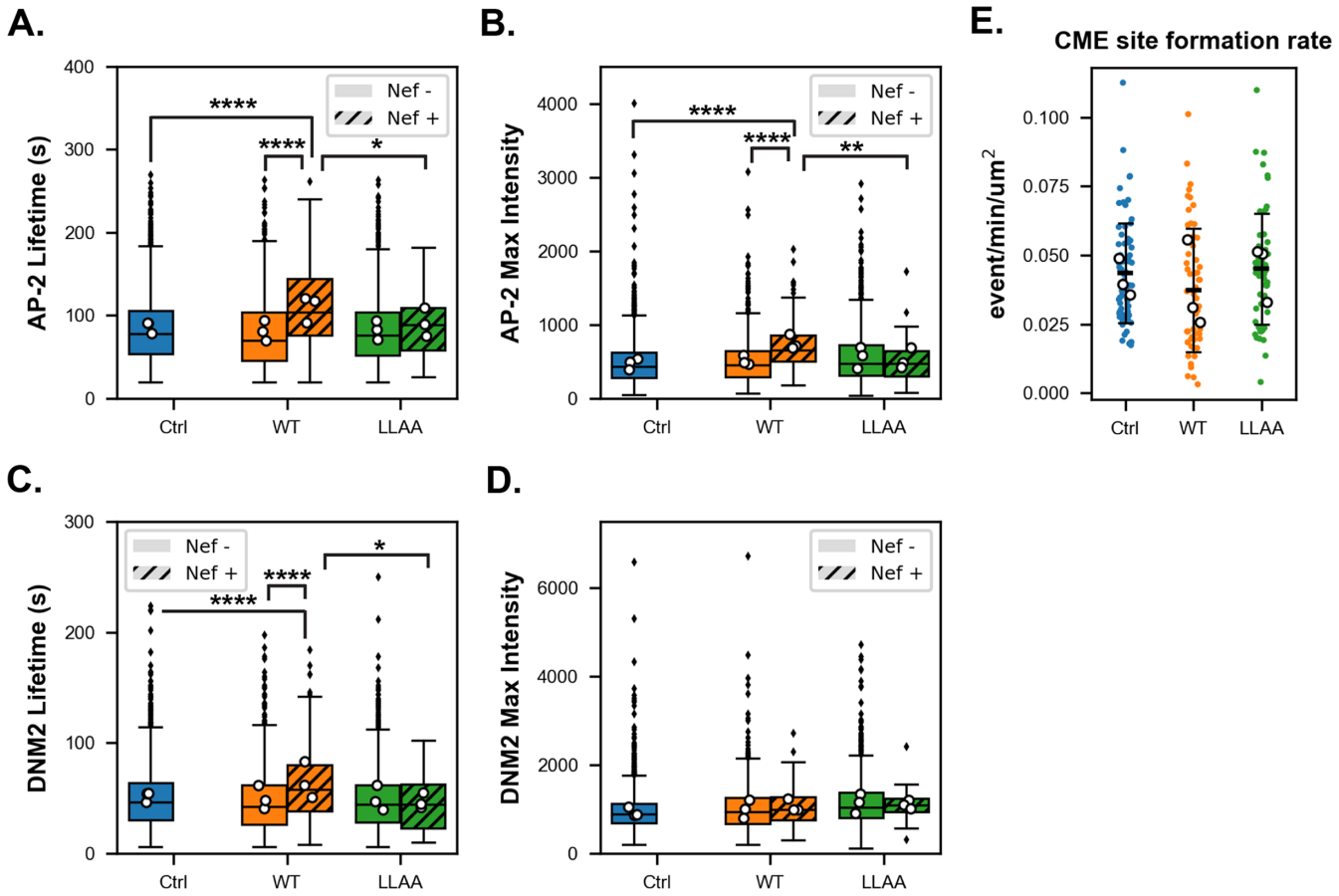

FIGURE 3: Nef+ CME sites display longer AP-2 and DNM2 lifetimes and higher AP-2 maximum intensities. (A) Quantification of AP-2 lifetime as a boxplot. The control (ctrl) CME events are those observed in the parental AP-2-RFP and DNM2-GFP Jurkat cell line. WT and LLAA refers to WT Nef-transfected and dileucine motif mutated LLAA Nef-transfected cells, respectively. The Nef+ and Nef– CME events are those that recruit and do not recruit Nef in the Nef-expressing cell. Open circles represent mean values from biological replicates. (B) Quantification of AP-2 max intensity. Same data set as A. (C) Quantification of DNM2 lifetime. Same data set as A. (D) Quantification of DNM2 max intensity. Same data set as A. For A–D, *, **, **** indicates p value < 0.05, < 0.01, and < 0.0001, respectively. (E) Quantification of CME site formation in control, WT Nef-transfected, and LLAA Nef-transfected Jurkat cells. Each datapoint is an individual cell. Each open circle represents the mean value from a single biological replicate. Bars indicate SD.

(Figure 3, C and D). Taken together, these results indicate that Nef modulates the dynamics and level of CME protein recruitment to CME sites, likely through its dileucine motif-dependent interaction with AP-2.

Neither the number of Nef molecules at a CME site nor the total expression induction time predict AP-2 lifetime or the amount of AP-2 recruitment

To gain further insight into how Nef affects CME dynamics, we asked whether the amount of Nef recruited to a CME site predicts the magnitude of the observed phenotypes. We addressed this question by stably integrating an inducible form of HIV-Nef-HALO into the genome-engineered Jurkat cells to gain control over the duration and amount of Nef expression (Supplemental Figure S3, A and B; Supplemental Movie 6). Using the Nef-inducible cell line, Nef expression was induced for 0, 2, 4, 6, and 24 h to vary the amount of Nef recruitment to CME sites. Nef expression increased with longer induction time (Supplemental Figure S3, A and B), as did the amount of Nef recruited to Nef+ sites and the percent of Nef+ sites (Supplemental Figure S3, C and D). However, there was no detectable difference in AP-2 lifetime or AP-2 amount recruited at different times of Nef induction (Supplemental Figure S3, E and F). These results suggest that the threshold for the full effect of Nef recruitment on CME sites is low or that Nef-dependent effects on CME dynamics might require other factors.

Nef+ CME sites show increased endocytic productivity

Previous studies concluded that to varying degrees in different cell types, initiated CME events do not always proceed to productive vesicle formation. Characteristics of productive CME events include longer AP-2 lifetimes, higher AP-2 recruitment levels, and DNM2 recruitment in a sharp peak just before its disappearance (Ehrlich *et al.*, 2004; Loerke *et al.*, 2009; Taylor *et al.*, 2011; Aguet *et al.*, 2013; Hong *et al.*, 2015). We sought to determine whether the effects of Nef on CME protein recruitment levels and lifetime might reflect increased CME productivity.

One distinguishing feature of nonproductive, or abortive, CME events is that their AP-2 lifetimes are often less than ~20 s in length (Hong *et al.*, 2015). To this end, we first analyzed differences in AP-2

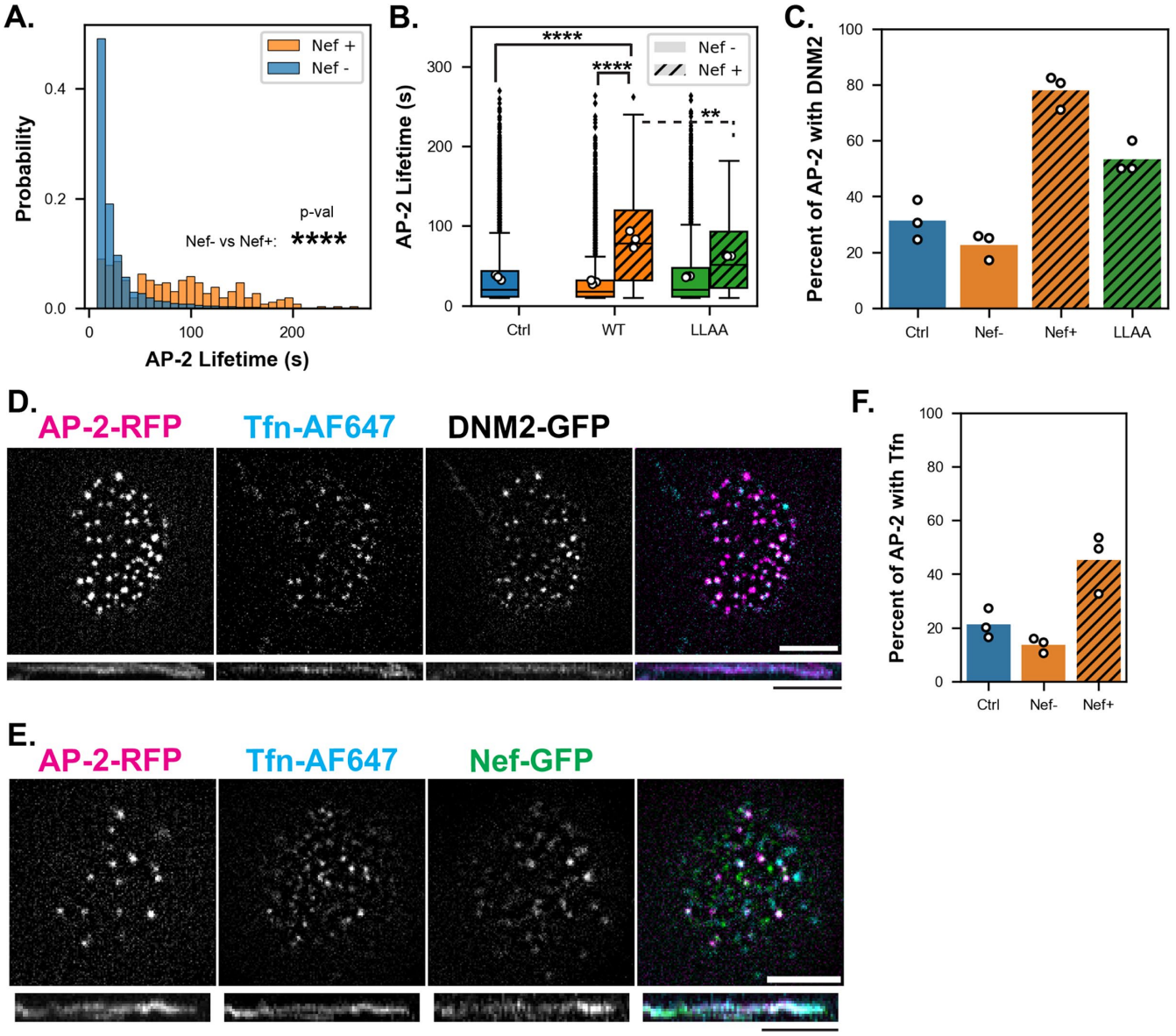

FIGURE 4: Nef recruitment correlates with DNM2 and transferrin recruitment at CME sites. (A) Quantification of AP-2 lifetime as a histogram. Dataset consists of all Nef+ and Nef– CME events in WT Nef-transfected cells, regardless of DNM2 recruitment. **** indicates p value < 0.0001. (B) Quantification of AP-2 lifetime as a barplot. Dataset consists of all events in untransfected, WT Nef and LLAA Nef–transfected cells, regardless of DNM2 recruitment. Open circles represent mean values from biological replicates. **, **** indicates p value <0.05 and < 0.0001, respectively. (C) Bar plot showing the fraction of AP-2 events to which DNM2 was recruited. Dataset consists of all events regardless of DNM2 recruitment from untransfected, WT Nef, or LLAA Nef–transfected Jurkat cells. Datapoints represent percentage of events that recruit DNM2 from separate biological replicates. (D) TIRF image of AP-2-RFP, DNM2-GFP Jurkat cells labeled with Alexa Fluor 647 labeled transferrin (Tfn-AF647). Local background was reduced by subtracting the median filtered image to highlight punctate structures. Scale bar is 5 μm. Below, a sample kymograph of a CME event that exhibited Tfn-AF647 signal is shown. Scale bar is 1 min. (E) TIRF image of AP-2-RFP Jurkat cells transfected with WT Nef-GFP and labeled with Alexa Fluor 647 labeled transferrin (Tfn-AF647). Local background was reduced by subtracting the median filtered image to highlight punctate structures. Scale bar is 5 μm. Below, a sample kymograph of a CME event that exhibited Tfn-AF647 signal is shown. Scale bar is 1 min. (F) Bar plot showing the fraction of AP-2 events at which transferrin was recruited. Datapoints represent percentage of events that recruit transferrin from separate biological replicates.

lifetimes for Nef+ and Nef– events through generation of histograms for AP-2 lifetimes of all detected dynamic events, regardless of whether these events concluded with DNM2 recruitment (Figure 4A). Strikingly, the histogram for Nef– events reveals predominantly short-lived AP-2 events, while the histogram for Nef+ events reveals a much larger fraction of CME events with longer AP-2 lifetimes. Furthermore, control CME events showed a similar AP-2 lifetime distribution to Nef– events, while LLAA Nef+ events showed an intermediate AP-2 lifetime distribution (Figure 4B). Together, these observations indicate that Nef+ events are much less likely to exhibit AP-2 lifetimes of less than 20 s, and that this effect is partially dependent on the interaction between Nef and AP-2.

We assessed the productivity of Nef+ events by comparing the fraction of Nef+ events that recruited DNM2 to the Nef– and control events that recruited DNM2. Because DNM2 is also recruited at low levels during early CME, we included a minimum DNM2 intensity threshold based on the DNM2 max intensity for AP-2 events with lifetimes shorter than 20 s. DNM2 was recruited to 78% of Nef+ events and only 31 and 23% of control and Nef– events, respectively (Figure 4C). DNM2 was recruited to 53% of LLAA Nef+ events, showing an intermediate value consistent with the intermediate AP-2 lifetime increase observed for LLAA Nef+ events (Figures 3A and 4C). A much larger fraction of Nef+ CME sites recruit DNM2 compared with control, Nef–, and LLAA Nef+ sites.

To orthogonally test whether Nef recruitment increases CME site productivity, we monitored transferrin internalization from Nef ± CME sites since the successful capture of transferrin is associated with productive CME (Ehrlich *et al.*, 2004; Liu *et al.*, 2010). We were able to label CME sites by directly adding Alexa Fluor 647 (AF647)-labeled transferrin to plated Jurkat cells while imaging at 37°C without prior starvation or cooling, as was done previously by Ehrlich et al (2004). After less than a minute of incubation, the fluorescent transferrin molecules were visible as punctate structures at the bottom surface of the cell that colocalized with CME markers (Figure 4D; Supplemental Movie 7). To monitor both Nef and transferrin signal, we expressed GFP tagged NA7 Nef in AP2-RFP genome-edited Jurkat cells and incubated the cells with AF647-labeled transferrin. We observed that some Nef+ CME sites were labeled with transferrin, establishing that transferrin is recruited to Nef+ CME sites (Figure 4E; Supplemental Movie 8). Transferrin therefore could be used as a marker for CME productivity. Transferrin recruitment to CME sites was scored by its association with AP-2 puncta and by whether transferrin signal disappeared with or after the AP-2 signal. Using these criteria, we determined transferrin is recruited to 21 and 14% of control– and Nef– sites, while it is recruited to 45% of Nef+ events (Figure 4F).

In summary, these results suggest that Nef renders CME sites more productive than control or Nef– sites, in part through its dileucine motif-dependent interactions with AP-2.

DISCUSSION

Current literature supports a model in which HIV Nef downregulates CD4, SERINC5, and other membrane proteins from the cell surface by acting as an adaptor to connect AP-2 to the target cargo protein. Here, we closely examined the kinetic aspect of this model in a cell line that resembles the natural biological host of HIV and expresses endogenously tagged fluorescent derivatives of CME proteins AP-2 and dynamin2.

Nef specifically localizes to CME sites in Jurkat cells

Nef localized to CME sites in a dileucine motif-dependent manner in the genome-edited Jurkat cells, consistent with previous findings (Greenberg *et al.*, 1997, 1998; Burtey *et al.*, 2007). Of note, we observed low but clear localization of the dileucine motif mutated LLAA Nef at CME sites. Though the CME-dependent functions of Nef primarily rely on the direct interaction between the Nef dileucine motif and AP-2, our observation indicates the LLAA Nef mutant behaves in a hypomorphic manner rather than as a null mutant. In agreement with this conclusion, we observed intermediate phenotypes for LLAA Nef across several experiments in this study (AP-2 lifetime, DNM2 recruitment, Tfn recruitment). Mutation of the dileucine motif abolished Nef activity when assayed through flow cytometry and viral infectivity assays, suggesting LLAA Nef activity that we detected in this study would be insufficient to enhance HIV-1 infectivity (Jin *et al.*, 2005; Pizzato *et al.*, 2007). This raises an intriguing possibility that even partially disrupting Nef interaction with the CME pathway could have major effects on HIV-1 infectivity.

Many Nef puncta that do not colocalize with endocytic proteins were also observed. The dynamics of these structures did not change in a Nef dileucine motif-dependent manner and therefore might represent other sites of Nef recruitment on the plasma membrane such as lipid rafts (Wang *et al.*, 2000; Alexander *et al.*, 2004). Surprisingly, we detected more Nef puncta that did not colocalize with CME markers than was reported in a previous study (Burtey *et al.*, 2007). This difference might be due to use of different cell lines, presence of intracellular Nef compartments captured in the evanescent field of the TIRF scope, a difference in the sensitivity of the imaging systems used, or differences in the tracking parameters used for quantification of Nef and CME dynamics.

Nef recruitment to CME sites appears to be dependent on extracellular environment

We noticed that in the region of the plasma membrane that was not attached to the cover glass, almost all CME sites were dynamic, appearing and disappearing. Seven percent of CME sites on regions of the plasma membrane attached to the cover glass persisted for the entirety of our 5 minute movies. These persistent sites showed greatly increased Nef recruitment compared with dynamic sites. This observation is consistent with results from a previous study that reported increased colocalization of Nef and clathrin at persistent sites in HeLa cells (Burtey *et al.*, 2007). These persistent AP-2 structures have been proposed to form upon cell engagement with substrate by interacting with receptors such as integrins that bind the extracellular matrix to form cellular adhesions (Baschieri *et al.*, 2018). AP-2–positive clathrin-coated structures have been shown to wrap around extracellular matrix elements such as collagen (Elkhatib *et al.*, 2017). Because Nef was observed more frequently at these persistent CME sites, our data suggests that Nef recruitment to CME sites may be sensitive to contact between the infected-host cell and the extracellular environment.

Nef is recruited to endocytic sites early and displays dynamics similar to AP-2

Nef was typically detected at CME sites within the first 20 s of AP-2 detection (Figure 2C). After recruitment, the intensity of the Nef signal increased with a similar kinetic profile to that of AP-2, further supporting the conclusion that its recruitment is mediated by AP-2. We observed that the Nef signal usually persisted until the AP-2 signal was no longer detectable, suggesting that Nef was either internalized as a part of the clathrin-coated vesicle or dissociates close in time to scission. However, whether Nef persists on the endocytosed vesicle after uncoating is not clear, although we observed by HILO microscopy a few events wherein Nef remained associated with the endocytosed vesicle after AP-2 disappeared. Determining whether Nef remains on the endocytic vesicle after internalization will be important for understanding whether and/or how Nef modulates endocytic trafficking after internalization from the plasma membrane. There are likely additional windows of Nef-mediated traffic modulation downstream of CME in the endocytosis pathway that prevent recycling of Nef cargo given its extensive association with other trafficking proteins throughout the cell (Pereira and daSilva, 2016; Buffalo *et al.*, 2019a). Further investigation of this "hand-off" of Nef cargo throughout the endocytic trafficking pathway promises to provide novel insights into the mechanism of Nef-dependent host defense factor downregulation.

Nef increases CME protein lifetimes and AP-2 recruitment

Through particle-tracking analysis, we observed that AP-2 and dynamin2 lifetimes, as well as the maximal amount of AP-2 recruitment, were greater at Nef+ CME sites relative to Nef– sites in the same cells. Because Nef's effects on CME protein dynamics were detected at Nef+ CME sites but not at Nef- CME sites, we conclude that Nef acts on CME dynamics via direct interactions rather than long-range effects. Given the importance of the Nef dileucine motif in these Nef-dependent changes in CME dynamics, we propose a simple model wherein Nef increases AP-2 lifetime and recruitment by serving as an additional bridge between AP-2 and the plasma membrane through its dileucine motif and N-terminal membrane binding domain. Additionally, binding between dynamin2 and Nef might increase dynamin2's lifetime at CME sites (Pizzato *et al.*, 2007). In a previous study, Nef was shown to interact with dynamin2, and mutations that decrease or abolish this interaction were shown to reduce viral infectivity (Pizzato *et al.*, 2007). However, binding between dynamin2 and Nef was reported to be independent of the dileucine motif (Pizzato *et al.*, 2007). In our study, the increase in dynamin2 lifetime was dependent on the Nef dileucine motif, perhaps because Nef needs to be recruited to CME sites before binding to dynamin2. However, whether the interaction between dynamin2 and Nef plays a role in Nef-mediated CME pathway modulation remains inconclusive. An intriguing question is whether this interaction might work in concert with the interaction between AP-2 and Nef to further stabilize Nef at the CME site and/or to promote dynamin2 recruitment.

The lack of correlation between the amount of Nef recruited and AP-2 recruitment/lifetime was unexpected (Supplemental Figure S3, E and F). One possibility is that there is a low saturation threshold for Nef-dependent modulation of CME dynamics, so a few molecules of Nef are sufficient to produce the observed phenotypes. This low saturation threshold could be due to spatial restrictions of a clathrin-coated vesicle limiting the maximal amount of AP-2 accumulation or due to high potency of individual Nef molecules. An alternative possibility is that there is a local amplification of Nef effects at the CME site such that only a small amount of Nef is necessary to saturate the effect. Outside of its trafficking functions, Nef has been shown to modulate signaling through interaction with various kinases. For example, Nef activates Src family kinases through binding of Nef's proline-rich domain to the negative regulatory SH3 domains of Src family kinases (Saksela *et al.*, 1995). On the other hand, Nef mutations in the proline-rich domain involved in binding the SH3 domains of Src family kinases do not interfere with Nef's downregulation of CD4 through CME (Saksela *et al.*, 1995). Many CME proteins such as dynamin2 also interact through a multivalent SH3 and proline-rich domain network at the CME site, raising the possibility that the observed Nef-dependent changes might involve this network as well (Li *et al.*, 2012; Sun *et al.*, 2017). A third explanation for the lack of correlation between Nef levels and effects is the possibility that HIV Nef functions require additional factors such as cargo. HIV Nef, as well as the closely related SIV Nef has been shown to form a tripartite complex consisting of the AP-2 complex, the cytoplasmic tail of the target host cargo protein, and itself (Buffalo *et al.*, 2019b; Kwon *et al.*, 2020). The formation of such complexes maybe required for Nef to modulate CME dynamics. A mixed population of target-bound Nef and target-free Nef might explain the lack of strong correlation between the amount of Nef and the magnitude of its effect on CME.

Nef recruitment to CME sites might increase endocytic productivity

Finally, we obtained evidence suggesting that Nef increases CME site productivity. Nonproductive or abortive events are characterized by low accumulation of endocytic coat proteins and lack of late CME protein recruitment, such as the final burst of dynamin2 recruitment and subsequent arrival of uncoating factors (Ehrlich *et al.*, 2004; Aguet *et al.*, 2013; Hong *et al.*, 2015; He *et al.*, 2020). Here, we showed that Nef-positive CME sites have markedly increased AP-2 lifetimes and recruitment levels and are around 50% more likely to recruit detectable dynamin2 in a late peak. At most CME sites at which Nef is detected, Nef is detected at CME sites within 18 s of AP-2 detection, meaning that Nef is present within the lifetime of both abortive and productive events, the time window during which it could influence CME site productivity. Further supporting this possibility, we showed that a much larger fraction of Nef+ CME sites recruits transferrin molecules compared with control or Nef– CME sites. Importantly, the dileucine motif interaction between Nef and AP-2 is similar to the way in which some membrane receptors interact with AP-2 to be internalized (Kelly *et al.*, 2008; Ren *et al.*, 2014). Previous studies demonstrated that an increase in the local concentration of membrane proteins harboring the tyrosine motif, a different AP-2 binding motif, can increase CME productivity (Loerke *et al.*, 2009; Liu *et al.*, 2010; Kadlecova *et al.*, 2017). An analogous mechanism wherein the Nef dileucine motif mimics membrane protein binding to AP-2 might increase CME productivity in a similar manner.

In conclusion, we report here that Nef increases the recruitment and lifetimes of AP-2 and dynamin2 at CME sites. The effects of Nef on the AP-2 protein recruitment and lifetime were dependent on its dileucine motif. Nef+ CME sites exhibit increased productivity in a partially dileucine motif-dependent manner as well. Given these observations, we propose that Nef increases the recruitment and accumulation of AP-2 at CME sites via its dileucine motif, thereby increasing productivity through AP-2 stabilization and promoting membrane protein downregulation (Figure 5).

MATERIALS AND METHODS

Request a protocol through *Bio-protocol*.

Cloning

The donor vector for endogenously tagging the *dynamin2* gene was generated by fusing the pCR8 backbone, 5′ DNM2 homology arm, GTSGGS linker, tagGFP2, and 3′ DNM2 homology arm via Gibson assembly. The donor vector for endogenously tagging the *AP2M1* gene was generated by fusing the pCR8 backbone, 5′ AP-2 homology arm, GTSGGS linker, tagRFPt, GMDELYKASGSGT linker, and 3′ AP-2 homology arm via Gibson assembly. Homology arms of genes were obtained from genomic PCR. NA7-Nef-HALO was generated by fusing the pcDNA5 backbone with the codon-optimized coding sequence of the NA7 Nef (protein ID: ABB51086.1), SGGTG linker, and HALO tag via Gibson assembly. The NA7-Nef-GFP plasmid was generated by replacing the HALO tag with a EGFP tag via Gibson assembly. The pcDNA5 NA7-Nef-HALO LLAA construct was generated by mutating L164 and L165 into alanines via site-directed mutagenesis from the pcDNA5 NA7-Nef-HALO construct. The pInducer20 NA7-Nef-HALO was generated by cloning the NA7-Nef-HALO insert into the pENTR1A vector, followed by gateway assembly of the insert into the pInducer20 packaging vector (Meerbrey *et al.*, 2011).

Cell culture

Experiments were conducted using Jurkat E6-1 cells, originally obtained from the UCB Cell Culture Facility. The cells were cultured in RPMI-1640 Media supplemented with 10% fetal bovine serum (FBS), Pen-Strep, and Sodium Pyruvate and grown at 37°C and 5% CO_2. Cells were maintained at densities below 2×10^6 cells/ml during passaging and experiments were conducted within 20 passages

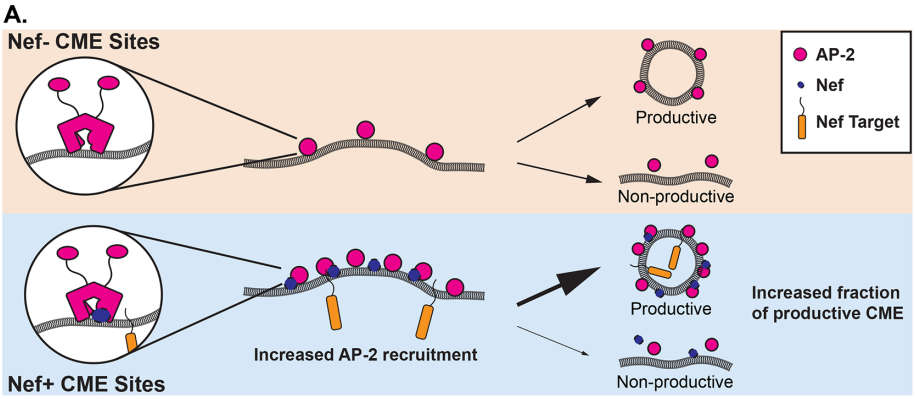

FIGURE 5: Model for the Nef mediated hijack of CME protein dynamics. (A) Model for how Nef recruitment modifies CME kinetics. At Nef+ sites, Nef increases AP-2 recruitment. The Nef+ CME sites show increased productivity, meaning that more sites mature to vesicles with more AP-2 and presumably more cargo, resulting in more efficient internalization of Nef target proteins through CME.

from the generation of the cell line. Stable cell lines inducibly expressing Nef were selected with G418 concentration of 800 µg/ml and maintained with concentration of 400 µg/ml. For lentiviral production, HEK293T cells were cultured in DMEM/F-12 media supplemented with 10% FBS, Pen-Strep, and nonessential amino acids on 10-cm plates.

Jurkat cells were obtained from the Berkeley Cell Culture Facility. STR profiling of AP2-RFP, DNM2-GFP, and AP2-RFP, DNM2-GFP, NA7-HALO Jurkat cell lines was conducted for cell-line authentication. Cell lines were tested for mycoplasma before use in microscopy experiments.

Electroporation

For genome editing, Jurkat cells were electroporated using the Amaxa Nucleofector 2b, protocol X-01. For transient transfections, Jurkat cells were electroporated using the Ingenio electroporation solution following the manufacturer's instructions (Mirus 50111). Electroporation was conducted using the Biorad Gene Pulser Xcell System using 0.4-cm cuvettes. $1 \times 10^6 - 2 \times 10^6$ Jurkat cells were transfected per condition. The settings for the electroporation used were voltage of 180, pulse length of 10 ms, and single pulse.

Genome editing

Jurkat cells were genome-edited by electroporation of the Cas9-crRNAtracrRNA complex using the Amaxa Nucleofector 2 b electroporator. Donor vectors for genome-editing have homology arms ranging from 700–1000 bp, and were electroporated with the Cas9 complex. The gRNA sequence TTGCTTCCCGCTGCAAGCAG was used to target *AP2M1*, and the gRNA sequence CCTGCTCGACTAGGCCTCGA was used to target *DNM2*. Jurkat cells were cultured for 3 d after electroporation and sorted into 96-well plates for clonal expansion using fluorescent signal to isolate edited clones using the BD Bioscience Influx sorter (BD Biosciences). Both alleles of AP-2 and one allele of DNM2 were tagged in the final cell line.

The *Streptococcus Pyogenes* NLS-Cas9 was purified in the University of California Berkeley QB3 Macrolab. Sorting was conducted in the University of California Berkeley CRL flow cytometry facility.

Lentiviral production and infection

The pInducer20-NA7-Nef-Halo vector was packaged into lentiviruses in HEK293T cells by cotransfection with second-generation lentiviral packaging plasmids (Addgene 182993 and 244397) using TransIT-LT1 transfection reagent according to the manufacturer's instructions (Mirus 2304). Viral supernatants were collected for 3 d and filtered through a 0.45-µm polyethersulfone filter. The collected supernatant was concentrated with LentiX concentrator following the manufacturer's instructions (Takara 631232). The virus containing pellet was then resuspended in 1 ml of the supernatant and stored in 100 µl aliquots at −80°C.

To generate stable Jurkat cell lines, Jurkat cells were subcultured in a well of a 6-well plate. An aliquot of the concentrated virus was directly pipetted into the well and cells were incubated with virus overnight. The following day, the media was replaced with media containing 800 µg/ml G418 for selection. The infected Jurkat cells were selected in G418 for 2 wk before use in experiments. After 2 wk, the stable Jurkat cell lines were cultured in 400 µg/ml G418.

Live-cell microscopy

Jurkat cells were incubated with 100 nM JF635 dye at least 1 h before imaging whether expressing or being compared with cell lines expressing HALO-tagged proteins. NA7 Nef expression was induced by treating cells with 0.1 µg/ml Doxycycline for the desired duration. AP-2-RFP DNM2-GFP and the uninduced AP-2-RFP DNM2-GFP NA7-Nef-HALO Jurkat cell lines were incubated with an equal volume of DMSO instead for 24 h.

All imaging was conducted on eight well-chambered glass slides (Cellvis C8-1.5H-N), coated with 1 mg/ml Poly-L-Lysine. Plates were coated for 10 min and washed three times with phosphate-buffered saline (PBS). Jurkat cells were transferred to imaging media (growth media without phenol red) and allowed to adhere on the well for 10 min before imaging.

Images were acquired through TIRF microscopy using a Nikon Ecliplse Ti2 inverted microscope. The TIRF scope was equipped with a LUNF 4-line laser launch (Nikon Instruments) and an iLas2 RING-TIRF module (Gataca Systems). The CFI60 60× Apo TIRF objective and a Hamamatsu Orca Fusion Gen III sCMOS camera were used to capture images. All movies were acquired at 37°C sequentially over 5 min at 2 s intervals and 100 ms exposure for each channel. The system was controlled with NIS-Elements software.

For HILO microscopy, Jurkat cells were prepared as described and the excitation laser was angled at 55 degrees. The plane chosen for imaging was the focal plane closest to the bottom of the coverslip where fluorescence from the bottom surface of the cell could not be observed. The incubation condition and other imaging parameters were the same as in TIRF.

All datasets consist of three movies per condition per day, taken on three separate days. Specific numbers of cells and tracks (detected CME events) can be found in Table 1.

Transferrin labeling

Cells were labeled with Alexa Fluor 647–conjugated transferrin (Jackson ImmunoResearch 009-600-050) following a similar protocol to that used in Ehrlich *et al.* (2004). Briefly, Jurkat cells were incubated with Alexa Fluor 647-conjugated transferrin at a concentration of 1 µg/ml. The mixture was incubated on a Poly-L-Lysine

Data set	Imaging Sessions	Movies	Cells	Tracks (events)	Nef–	Nef+	All tracks	Persistent
TIRF Nef transfection experiment								
Control (Untransfected)	3	9	73				12,741	970
WT Nef	3	9	55				8292	788
LLAA Nef	3	9	58				9226	801
Dynamic CME tracks								
Control (Untransfected)				2115	2115	0		
WT Nef				1074	913	161		
LLAA Nef				1356	1334	22		
Dynamic all tracks								
Control (Untransfected)				9155	9155	0		
WT Nef				6703	6454	249		
LLAA Nef				5431	5384	47		
Nef tracks								
WT Nef				26011				
LLAA Nef				26617				
HILO Nef transfection experiment (Dynamic CME tracks)								
Control (Untransfected)	3	9		85	85	0	699	2
WT Nef	3	9	41	205	161	44		
LLAA Nef	3	9	34	161	147	14		
TIRF Nef induction experiment (Dynamic CME tracks)								
Control (Parental Cell Line)	3	9	140	3006	3006	0		
0 h induction	3	9	169	4577	4466	111		
2 h induction	3	9	157	3332	3197	135		
4 h induction	3	10	141	2684	2505	179		
6 h induction	3	9	148	2711	2398	313		
24 h induction	3	10	146	2510	2270	240		
TIRF Tfn uptake experiment (Dynamic CME tracks)					Nef–	Nef+	Tfn–	Tfn+
AP2-RFP, DNM2-GFP	3	9	50	649	649	0	456	193
AP2-RFP	3	10	26	5719	5719	0	5158	561
AP2-RFP, WT Nef-HALO	3	13	29	5365	4989	376	4895	470

TABLE 1: The sample size for datasets used in study.

imaging well for 5 min before imaging. Cells were kept at 37°C without prior starvation during the labeling process.

Cell lysis and Western blot

$1 \times 10^6 - 2 \times 10^6$ Jurkat cells were washed with PBS and resuspended in 24 µl of lysis buffer, consisting of 50 mM HEPES pH 7.4, 150 mM NaCl, 1 mM $MgCl_2$, 1% NP40, phosSTOP (Roche 4906845001), and protease inhibitor (Roche 1183617001). Cells were lysed for 15 min on ice with gentle agitation every 5 min. Lysed cells were then centrifuged at 4°C and 13,000 rpm for 15 min. 18 µl of the supernatant was collected as lysate. The lysate was mixed with Laemmeli reducing buffer with 5% β-mercaptoethanol. 10 µl of the final solution was loaded onto a 10% acrylamide gel for SDS–PAGE analysis. Proteins resolved on the SDS–PAGE gel was transferred onto a nitrocellulose membrane for immunoblotting via wet transfer. Blots were blocked with 5% milk in tris-buffered saline (TBS) and incubated with primary antibody. The antibodies used for Western blotting were: anti-HALO (1:1000 in 0.5% milk TBST (Tris-buffered saline with 0.1% Tween 20), 4°C o/n, Promega G9211), anti-GAPDH (1:10,000 in TBST, room temperature [RT] 1 h, ab9485), anti-AP-2M1 (1:500 in 0.5% milk TBST, 4°C o/n, Abcam, ab75995), and anti-Tag(CGY)FP (1:2000 in 0.5% milk TBST, 4°C o/n, Evrogen AB121). Blots were then incubated with IRDye 800/680–conjugated antibodies (1:10,000 in 5% milk TBST, RT 1 h, 926-32212 926-68071) and imaged on the LICOR Odyssey scanner.

Image processing

Before kymograph and colocalization analysis through imageJ, images were background subtracted (subtract mean value of box outside cell from all pixels), corrected for photobleaching if

applicable (Fiji bleach correction, exponential fitting method), and cytoplasmic background subtracted (Median filter, $r = 6$ px, was subtracted from image) to clearly visualize punctate structures.

Kymograph analysis of endocytic events

To create kymographs of midfocal plane imaging movies an average intensity Z-projection of these movies was generated and a drawing a 20-pixel wide line around circumference of cells. Intensity change of the movie within the line was projected across time. Lifetime measurements were made by drawing a horizontal line over the observed CME events in imageJ and measuring its length. The beginning and end of events were determined by when intensity levels were at least 3× background levels. Events were categorized as persistent if the AP-2 signal was present throughout the entire 5-min movie. Events were categorized as dynamic if the AP-2 signal appeared and disappeared within the 5-min movie.

Colocalization analysis

Colocalization was evaluated using three different methods. For HILO images, colocalization was manually assessed through kymograph analysis. For TIRF images, colocalization analysis for all events was conducted through imageJ. Individual cells were segmented into square regions with the cell in the center and separately assessed for colocalization. After processing, average intensity projections were generated for each channel. Masks for punctate structures were generated using the imageJ "Find Maxima" function (prominence setting of 10, with tolerance). The pixel overlap of the resulting masks was assessed for pairs of channels to test for colocalization. As a negative control, the mask generated from the AP-2 coat channel was rotated 90 degrees and compared with masks from other channels, establishing a baseline for chance colocalization. See Supplemental Figure S4, A–C.

Particle tracking analysis

For particle tracking analysis, cells were cropped individually and separated into cell-specific folders for analysis using the cmeAnalysis MATLAB package (Aguet *et al.*, 2013). For tracking, gaussian PSF model fitting detection with a gap length of 2 (maximum number of frames that signal can be undetected within a track), tracking minimum radius of 3 (minimum radius for a group of pixels to be considered an event for tracking), and tracking maximum radius of 6 (maximum radius for a group of pixels to be considered an event for tracking). Tracks that showed an AP-2 lifetime greater than 20 s, mean squared displacement < 0.02μm^2, and at least three consecutive significant (p value < 0.01) detections of DNM2 were considered valid tracks. Tracks that showed at least four consecutive significant (p value < 1×10^{-25}) detections of Nef that averaged within <1.25 pixels away from AP-2 were considered to be Nef+ tracks. These parameters for assessing Nef colocalization were determined by manually examining montages of detected Nef colocalization events, and by comparing the number of detected Nef+ events in WT Nef and LLAA Nef-transfected samples. Dynamic events and persistent events were filtered by analyzing category 1 and 4 tracks in the cmeAnalysis software, respectively. Category 1 tracks are tracked events that begin after the first frame and end before the last frame of the movie. Category 4 tracks are events that are already present in the first frame of the movie and persist until the last frame. Lifetimes of DNM2 and Nef were calculated with a tolerable gap length of 2. For figure 4, tracks were considered to be DNM2 positive if there were at least three consecutive significant detections of DNM2 as well as a DNM2 maximum intensity higher than the 75th percentile of CME events that are shorter than 20 s. Tracks were considered to be transferrin positive if there were at least four consecutive significant detections of transferrin and if the transferrin signal terminated with or after the associated AP-2 signal. These parameters are summarized in Supplemental Figure S4 F.

Formation rate analysis

For analyzing the formation of punctate structures, the area of the individually cropped cells from the particle tracking analysis pipeline was estimated. First, the max projection of the cropped cells was generated using the numpy max function. The resulting image was then blurred using a mean filter (specific parameters can be found in the python notebook). The image was then binarized using the otsu threshold function and the number of nonzero pixels in the image was calculated. The filter and otsu threshold functions are part of the scikit-image python software analysis package (scikit-image.org). The number of tracked events was then divided by the estimated area and the duration of the movie to solve for the formation rate. See Supplemental Figure S4, D and E.

Scripts used for image analysis (Code Availability)

All user-made scripts for imageJ, MATLAB, and python can be accessed here: https://github.com/yuichiro-iwamoto/Nef-CME-analysis

Statistical analysis

Statistical analysis was performed by using the python package sciPy or with Prism 9. Nonparametric statistical tests were used to evaluate significance so no assumption about data distributions were made. Specifically, Mann–Whitney's U test was used to evaluate significance of two groups and the Kruskal–Wallis test was used to evaluate significance when multiple comparisons were made. For colocalization analysis, each cell imaged was considered to be an independent replicate. For dynamics-related analysis, each track was considered to be an independent replicate. Data were visualized using the python package seaborn and Prism 9. All reported values are indicated as mean ± SD.

ACKNOWLEDGMENTS

We thank Xuefeng Ren for generating the NA7 Nef construct, Frank Kirchhoff for helpful suggestions and Jonathan Wong for critical reading of the manuscript. This research was supported by National Institutes of Health grants R01 AI120691 (J.H.H.), P50 AI150476 (D.G.D. and J.H.H.), National Institute of General Medical Sciences (NIGMS) grant R35 GM118149 to D.G.D.

REFERENCES

Abraham RT, Weiss A (2004). Jurkat T cells and development of the T-cell receptor signalling paradigm. Nat Rev Immunol 4, 301–308.

Aguet F, Antonescu CN, Mettlen M, Schmid SL, Danuser G (2013). Advances in analysis of low signal-to-noise images link dynamin and AP2 to the functions of an endocytic checkpoint. Dev Cell 26, 279–291.

Aiken C, Konner J, Landau NR, Lenburg ME, Trono D (1994). Nef induces CD4 endocytosis: requirement for a critical dileucine motif in the membrane-proximal CD4 cytoplasmic domain. Cell 76, 853–864.

Alexander M, Bor YC, Ravichandran KS, Hammarskjold ML, Rekosh D (2004). Human immunodeficiency virus type 1 Nef associates with lipid rafts to downmodulate cell surface CD4 and class I major histocompatibility complex expression and to increase viral infectivity. J Virol 78, 1685–1696.

Allan JS, Coligan JE, Lee TH, McLane MF, Kanki PJ, Groopman JE, Essex M (1985). A new HTLV-III/LAV encoded antigen detected by antibodies from AIDS patients. Science 230, 810–813.

Antonny B, Burd C, De Camilli P, Chen E, Daumke O, Faelber K, Ford M, Frolov VA, Frost A, Hinshaw JE, *et al.* (2016). Membrane fission by dynamin: what we know and what we need to know. EMBO J 35, 2270–2284.

Baschieri F, Dayot S, Elkhatib N, Ly N, Capmany A, Schauer K, Betz T, Vignjevic DM, Poincloux R, Montagnac G (2018). Frustrated endocytosis

controls contractility-independent mechanotransduction at clathrin-coated structures. Nat Commun 9, 3825.
Basmaciogullari S, Pizzato M (2014). The activity of Nef on HIV-1 infectivity. Front Microbiol 5, 232.
Batchelder EM, Yarar D (2010). Differential requirements for clathrin-dependent endocytosis at sites of cell-substrate adhesion. Mol Biol Cell 21, 3070–3079.
Boucrot E, Saffarian S, Zhang R, Kirchhausen T (2010). Roles of AP-2 in clathrin-mediated endocytosis. PLoS One 5, e10597.
Bucher D, Frey F, Sochacki KA, Kummer S, Bergeest JP, Godinez WJ, Krausslich HG, Rohr K, Taraska JW, Schwarz US, Boulant S (2018). Clathrin-adaptor ratio and membrane tension regulate the flat-to-curved transition of the clathrin coat during endocytosis. Nat Commun 9, 1109.
Buffalo CZ, Iwamoto Y, Hurley JH, Ren X (2019a). How HIV Nef proteins hijack membrane traffic to promote infection. J Virol 93, e01322-19.
Buffalo CZ, Sturzel CM, Heusinger E, Kmiec D, Kirchhoff F, Hurley JH, Ren X (2019b). Structural basis for tetherin antagonism as a barrier to zoonotic lentiviral transmission. Cell Host Microbe 26, 359–368 e358.
Burtey A, Rappoport JZ, Bouchet J, Basmaciogullari S, Guatelli J, Simon SM, Benichou S, Benmerah A (2007). Dynamic interaction of HIV-1 Nef with the clathrin-mediated endocytic pathway at the plasma membrane. Traffic 8, 61–76.
Chaudhuri R, Lindwasser OW, Smith WJ, Hurley JH, Bonifacino JS (2007). Downregulation of CD4 by human immunodeficiency virus type 1 Nef is dependent on clathrin and involves direct interaction of Nef with the AP2 clathrin adaptor. J Virol 81, 3877–3890.
Cocucci E, Aguet F, Boulant S, Kirchhausen T (2012). The first five seconds in the life of a clathrin-coated pit. Cell 150, 495–507.
Cocucci E, Gaudin R, Kirchhausen T (2014). Dynamin recruitment and membrane scission at the neck of a clathrin-coated pit. Mol Biol Cell 25, 3595–3609.
Collins DR, Collins KL (2014). HIV-1 accessory proteins adapt cellular adaptors to facilitate immune evasion. PLoS Pathog 10, e1003851.
Deacon NJ, Tsykin A, Solomon A, Smith K, Ludford-Menting M, Hooker DJ, McPhee DA, Greenway AL, Ellett A, Chatfield C, *et al*. (1995). Genomic structure of an attenuated quasi species of HIV-1 from a blood transfusion donor and recipients. Science 270, 988–991.
Doyon JB, Zeitler B, Cheng J, Cheng AT, Cherone JM, Santiago Y, Lee AH, Vo TD, Doyon Y, Miller JC, *et al*. (2011). Rapid and efficient clathrin-mediated endocytosis revealed in genome-edited mammalian cells. Nat Cell Biol 13, 331–337.
Ehrlich M, Boll W, Van Oijen A, Hariharan R, Chandran K, Nibert ML, Kirchhausen T (2004). Endocytosis by random initiation and stabilization of clathrin-coated pits. Cell 118, 591–605.
Elkhatib N, Bresteau E, Baschieri F, Rioja AL, van Niel G, Vassilopoulos S, Montagnac G (2017). Tubular clathrin/AP-2 lattices pinch collagen fibers to support 3D cell migration. Science 356, eaal4713.
Grassart A, Cheng AT, Hong SH, Zhang F, Zenzer N, Feng Y, Briner DM, Davis GD, Malkov D, Drubin DG (2014). Actin and dynamin2 dynamics and interplay during clathrin-mediated endocytosis. J Cell Biol 205, 721–735.
Greenberg ME, Bronson S, Lock M, Neumann M, Pavlakis GN, Skowronski J (1997). Co-localization of HIV-1 Nef with the AP-2 adaptor protein complex correlates with Nef-induced CD4 down-regulation. EMBO J 16, 6964–6976.
Greenberg M, DeTulleo L, Rapoport I, Skowronski J, Kirchhausen T (1998). A dileucine motif in HIV-1 Nef is essential for sorting into clathrin-coated pits and for downregulation of CD4. Curr Biol 8, 1239–1242.
Guy B, Kieny MP, Riviere Y, Le Peuch C, Dott K, Girard M, Montagnier L, Lecocq JP (1987). HIV F/3′ orf encodes a phosphorylated GTP-binding protein resembling an oncogene product. Nature 330, 266–269.
He K, Song E, Upadhyayula S, Dang S, Gaudin R, Skillern W, Bu K, Capraro BR, Rapoport I, Kusters I, *et al*. (2020). Dynamics of Auxilin 1 and GAK in clathrin-mediated traffic. J Cell Biol 219, e201908142.
Hong SH, Cortesio CL, Drubin DG (2015). Machine-Learning-Based Analysis in Genome-Edited Cells Reveals the Efficiency of Clathrin-Mediated Endocytosis. Cell Rep 12, 2121–2130.
Inoue M, Koga Y, Djordjijevic D, Fukuma T, Reddy EP, Yokoyama MM, Sagawa K (1993). Down-regulation of CD4 molecules by the expression of Nef: a quantitative analysis of CD4 antigens on the cell surfaces. Int Immunol 5, 1067–1073.
Jia B, Serra-Moreno R, Neidermyer W, Rahmberg A, Mackey J, Fofana IB, Johnson WE, Westmoreland S, Evans DT (2009). Species-specific activity of SIV Nef and HIV-1 Vpu in overcoming restriction by tetherin/BST2. PLoS Pathog 5, e1000429.
Jin YJ, Cai CY, Zhang X, Zhang HT, Hirst JA, Burakoff SJ (2005). HIV Nef-mediated CD4 down-regulation is adaptor protein complex 2 dependent. J Immunol 175, 3157–3164.
Kadlecova Z, Spielman SJ, Loerke D, Mohanakrishnan A, Reed DK, Schmid SL (2017). Regulation of clathrin-mediated endocytosis by hierarchical allosteric activation of AP2. J Cell Biol 216, 167–179.
Kaksonen M, Sun Y, Drubin DG (2003). A pathway for association of receptors, adaptors, and actin during endocytic internalization. Cell 115, 475–487.
Kelly BT, McCoy AJ, Spate K, Miller SE, Evans PR, Honing S, Owen DJ (2008). A structural explanation for the binding of endocytic dileucine motifs by the AP2 complex. Nature 456, 976–979.
Kestler HW, 3rd, Ringler DJ, Mori K, Panicali DL, Sehgal PK, Daniel MD, Desrosiers RC (1991). Importance of the nef gene for maintenance of high virus loads and for development of AIDS. Cell 65, 651–662.
Kirchhoff F, Greenough TC, Brettler DB, Sullivan JL, Desrosiers RC (1995). Brief report: absence of intact nef sequences in a long-term survivor with nonprogressive HIV-1 infection. N Engl J Med 332, 228–232.
Kwon Y, Kaake RM, Echeverria I, Suarez M, Karimian Shamsabadi M, Stoneham C, Ramirez PW, Kress J, Singh R, Sali A, *et al*. (2020). Structural basis of CD4 downregulation by HIV-1 Nef. Nat Struct Mol Biol 27, 822–828.
Li P, Banjade S, Cheng HC, Kim S, Chen B, Guo L, Llaguno M, Hollingsworth JV, King DS, Banani SF, *et al*. (2012). Phase transitions in the assembly of multivalent signalling proteins. Nature 483, 336–340.
Liu AP, Aguet F, Danuser G, Schmid SL (2010). Local clustering of transferrin receptors promotes clathrin-coated pit initiation. J Cell Biol 191, 1381–1393.
Loerke D, Mettlen M, Yarar D, Jaqaman K, Jaqaman H, Danuser G, Schmid SL (2009). Cargo and dynamin regulate clathrin-coated pit maturation. PLoS Biol 7, e57.
Lu R, Drubin DG, Sun Y (2016). Clathrin-mediated endocytosis in budding yeast at a glance. J Cell Sci 129, 1531–1536.
Malim MH, Bieniasz PD (2012). HIV Restriction Factors and Mechanisms of Evasion. Cold Spring Harb Perspect Med 2, a006940.
Mariani R, Kirchhoff F, Greenough TC, Sullivan JL, Desrosiers RC, Skowronski J (1996). High frequency of defective nef alleles in a long-term survivor with nonprogressive human immunodeficiency virus type 1 infection. J Virol 70, 7752–7764.
Mariani R, Skowronski J (1993). CD4 down-regulation by nef alleles isolated from human immunodeficiency virus type 1-infected individuals. Proc Natl Acad Sci USA 90, 5549–5553.
Meerbrey KL, Hu G, Kessler JD, Roarty K, Li MZ, Fang JE, Herschkowitz JI, Burrows AE, Ciccia A, Sun T, *et al*. (2011). The pINDUCER lentiviral toolkit for inducible RNA interference in vitro and in vivo. Proc Natl Acad Sci USA 108, 3665–3670.
Merrifield CJ, Feldman ME, Wan L, Almers W (2002). Imaging actin and dynamin recruitment during invagination of single clathrin-coated pits. Nat Cell Biol 4, 691–698.
Pereira EA, daSilva LL (2016). HIV-1 Nef: Taking Control of Protein Trafficking. Traffic 17, 976–996.
Pizzato M, Helander A, Popova E, Calistri A, Zamborlini A, Palu G, Gottlinger HG (2007). Dynamin 2 is required for the enhancement of HIV-1 infectivity by Nef. Proc Natl Acad Sci USA 104, 6812–6817.
Ren X, Park SY, Bonifacino JS, Hurley JH (2014). How HIV-1 Nef hijacks the AP-2 clathrin adaptor to downregulate CD4. eLife 3, e01754.
Rosa A, Chande A, Ziglio S, De Sanctis V, Bertorelli R, Goh SL, McCauley SM, Nowosielska A, Antonarakis SE, Luban J, *et al*. (2015). HIV-1 Nef promotes infection by excluding SERINC5 from virion incorporation. Nature 526, 212–217.
Saksela K, Cheng G, Baltimore D (1995). Proline-rich (PxxP) motifs in HIV-1 Nef bind to SH3 domains of a subset of Src kinases and are required for the enhanced growth of Nef+ viruses but not for down-regulation of CD4. EMBO J 14, 484–491.
Schwartz O, Marechal V, Le Gall S, Lemonnier F, Heard JM (1996). Endocytosis of major histocompatibility complex class I molecules is induced by the HIV-1 Nef protein. Nat Med 2, 338–342.
Schwenk HU, Schneider U (1975). Cell cycle dependency of a T-cell marker on lymphoblasts. Blut 31, 299–306.
Serra-Moreno R, Zimmermann K, Stern LJ, Evans DT (2013). Tetherin/BST-2 antagonism by Nef depends on a direct physical interaction between Nef and tetherin, and on clathrin-mediated endocytosis. PLoS Pathog 9, e1003487.

Sun Y, Leong NT, Jiang T, Tangara A, Darzacq X, Drubin DG (2017). Switch-like Arp2/3 activation upon WASP and WIP recruitment to an apparent threshold level by multivalent linker proteins in vivo. eLife 6, e29140.
Taylor MJ, Perrais D, Merrifield CJ (2011). A high precision survey of the molecular dynamics of mammalian clathrin-mediated endocytosis. PLoS Biol 9, e1000604.
Tokunaga M, Imamoto N, Sakata-Sogawa K (2008). Highly inclined thin illumination enables clear single-molecule imaging in cells. Nat Methods 5, 159–161.
Usami Y, Wu Y, Gottlinger HG (2015). SERINC3 and SERINC5 restrict HIV-1 infectivity and are counteracted by Nef. Nature 526, 218–223.
Wang JK, Kiyokawa E, Verdin E, Trono D (2000). The Nef protein of HIV-1 associates with rafts and primes T cells for activation. Proc Natl Acad Sci USA 97, 394–399.
Zhang F, Wilson SJ, Landford WC, Virgen B, Gregory D, Johnson MC, Munch J, Kirchhoff F, Bieniasz PD, Hatziioannou T (2009). Nef proteins from simian immunodeficiency viruses are tetherin antagonists. Cell Host Microbe 6, 54–67.